Investigation of water jet breakup by supersonic rocket exhaust

Hansen Jones*, Vaibhav Rajora†, Shyam Menon‡

Louisiana State University, Baton Rouge, LA, 70808

In the testing of today's rocket engines, both on large scale vertical test stands and smaller subscale horizontal component testing stands, it is extremely important to accurately be able to quantify and mitigate the thermal and acoustic loads the engines will generate on test stand infrastructure. Due to the large number of parameters that must be considered for many cases, development of a multi-phase computational code is under way in order to properly analyze and design water spray cooling systems used at NASA's Stennis Space Center and across other NASA centers. A better understanding of the behavior and optimization of these systems would lead to a decrease in the cost of new systems and increase in the reliability of systems currently available. As such, a subscale test facility is being developed at Louisiana State University to provide experimental results which can be used to inform the development and verify the validity of such a code. The interaction of a supersonic jet of air with one or more water jets is examined and characterized using several non-intrusive diagnostic methods; focusing color Schlieren photography as well as laser sheet visualization is used obtain qualitative information about air jet and water breakup characteristics and phased doppler particle anemometry is used to gain point-wise statistical information about water particle size and velocity. In addition, work towards the transition to the examination of a combusting flow case using a scaled hybrid rocket engine will be presented.

I. Introduction

Liquid and solid fuel rockets play a vital role in supporting NASA's space exploration missions. The development of rocket engine technology for NASA missions is critically dependent on testing efforts carried out at NASA's Stennis Space Center (SSC) in Hancock, MS. The facility has been engaged in testing of rockets for the Apollo mission, the Space Shuttle program, and is currently involved in testing of rocket engines designed for the Space Launch System (SLS). During the fired rocket tests, the restrained rocket produces thrust, which is measured. At the same time, structural integrity and systems operation are measured and verified. The rocket engine exhaust plume is directed towards a deflector plate, which directs it safely away from the test facility as shown in **Figure 1** [1].

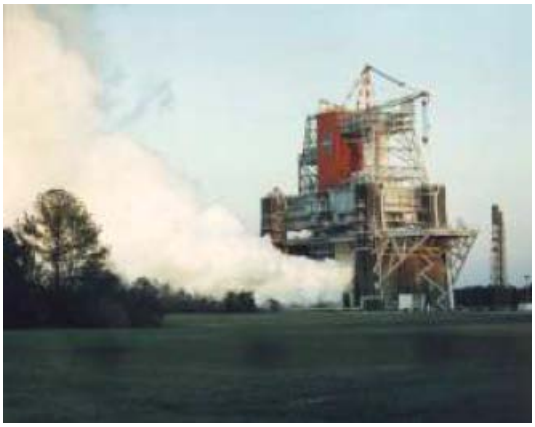

Figure 1: Space shuttle main engine undergoing test at the NASA Stennis B-1 test stand [1].

* Graduate Research Assistant, Mechanical and Industrial Engineering Department, hansen.j.jones@gmail.com
† Undergraduate Researcher, Department of Physics and Astronomy, vrajor1@lsu.edu
‡ Assistant Professor, Mechanical and Industrial Engineering Department, smenon@lsu.edu

The rocket exhaust plume has a complex structure and is characterized by an extreme environment with high temperature, high speed, supersonic flow. The plume has been proposed to be composed of an inviscid non-reactive core surrounded by a viscous mixing layer where reactions can take place by mixing with the ambient environment [2]. **Figure 2** shows CFD results by Allgood and Ahuja showing time-averaged temperature and Mach number iso-contours in the exhaust plume from the ARES-V rocket [3]. The temperature can be as high as 2600 K with an exit Mach number higher than 3. A considerable number of tests are required to ensure safe operation of the rocket. Each of these tests can have nominal burn times of the order of 480 s as is the case for the Space Shuttle Main Engine (SSME).

Frequently, it is also desired to evaluate rocket engine performance at altitude conditions. For such tests, the facilities employ a second-throat diffuser configuration as shown in **Figure 3** [4]. This setup uses the momentum of the exhaust gases to prevent backflow from the atmosphere into the test chamber [5]. This allows the rocket engine to be tested at the required vacuum pressure, which corresponds to the altitude for which the engine performance is being evaluated.

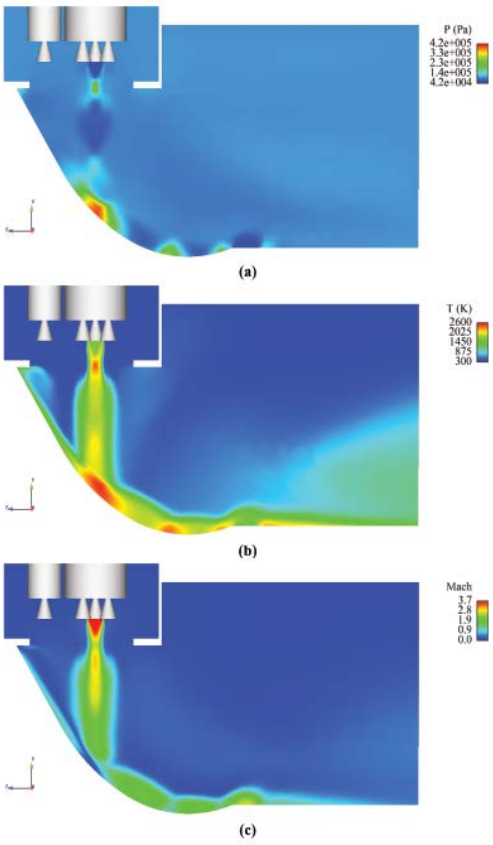

Figure 2: CFD results showing time-averaged iso-contours for pressure, temperature, and Mach number for the ARES V launch vehicle [3].

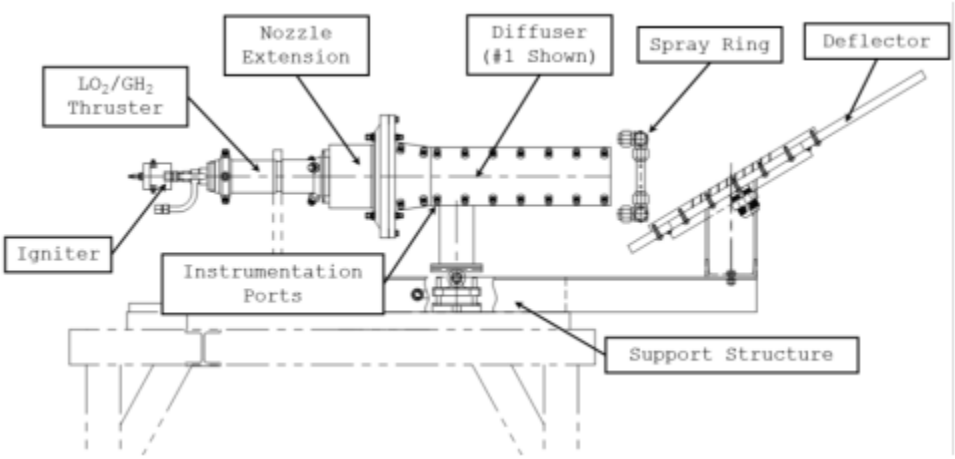

Figure 3: System schematic used in passive rocket diffuser testing at NASA Stennis [4].

For the types of rocket tests described above, it is critical to protect the infrastructure of the facility from the high temperature rocket exhaust flow. **Figure 4** (*left*) shows damage sustained by an uncooled flame trench following a test firing of an AJ26 engine. Thermal degradation and ejection of flame deflector material during testing commonly result in damage to the trench wall (**Figure 4** (*left*)) and should be avoided. Damage to the facility occurs due to thermal radiation heat transfer to the channels surrounding

the exhaust flow as well as due to direct heat transfer from the exhaust impinging on a deflector plate that the exhaust plume impinges on. The best approach to cool the large quantities of high velocity, high temperature exhaust from rocket plumes has been by spraying the exhaust with water using spray rings such as the one shown in **Figure 3**. Typical water flow rates range from 30 to 50 times the rocket weight flow rate [6]. **Figure 4** (*right*) shows the cooling ring used during static testing of the engine used on NASA's Morpheus lander. Large-scale test stands at NASA SSC are equipped to supply water flow rates in excess of 300,000 GPM. In addition to preventing thermal wear of the test facility components, water injection also serves a vital function of suppressing the noise produced by the supersonic exhaust [8]. In the test stands used at NASA SSC, the deflector plate is also equipped with arrays of water injection nozzles to reduce thermal degradation.

Figure 4: Left: Damage caused to uncooled flame trench, NASA SSC. April 26, 2017, Right: Water spray ring used to cool Morpheus engine static test [7].

There is a need to optimize the cooling system including the spray ring and the deflector plate to achieve maximum cooling efficiency with the least amount of water supply. This is a difficult problem to solve given the large number of free parameters such as plume impingement angle, water flow rate, nozzle injection diameter, and inlet pressure. This has led to the development of numerical simulations at NASA SSC to model the rocket exhaust plume and the water cooling system [3]. The simulations, which utilize a tightly coupled multi-phase computational framework can allow studies with large parametric variations to be performed in an efficient manner. However, the codes need to be validated to ensure accuracy and predictability. Reliable experimental data are required for a configuration, which encompasses all the relevant physics of the full-scale problem. This includes a high temperature, high speed, exhaust plume and two-phase interaction between the plume and cooling water jets. The experiment should be capable of providing accurate boundary conditions and measurements within the plume, which can be used to validate the codes.

Ongoing work is focused on developing a scaled hybrid rocket engine test apparatus to study the flow-field characteristics of an exhaust plume cooled by water injection. The setup when completed will allow for qualitative and quantitative measurements of the water spray cooling process. Currently, as a first step, a test campaign has been undertaken to analyze a similar setup in a cold flow configuration. This allows for the development of the test apparatus, fine tuning of the various diagnostic setups, and investigation of a configuration, which has seldom been studied in the past. Compressed air is used in lieu of the hybrid rocket to generate a high-speed exhaust plume and a single jet of water is injected into the plume. The resulting interaction between the supersonic plume with the water jet is studied using various diagnostic techniques. While the plume-jet interaction has some similarity to the well-studied subsonic jet in supersonic crossflow problem, there are also significant differences. This includes the absence of a solid boundary around the air

flow, which is replaced by a free boundary off which oblique shock waves and expansion waves are reflected. The water jet injected into this flow structure has more degrees of freedom in its motion as compared to the typical jet injected into a crossflow, which is constrained by solid boundaries.

Following the preceding discussion on the motivation for this work, the experimental methods and diagnostic techniques employed in this work are described in the following section. Test parameters covering the operating conditions of the experiment are detailed. This is followed by a description and analysis of the test results. Finally, conclusions and some directions for future work are described.

II. Experiment

A. Design of Experiment

The experiment is designed to produce a water spray by having a water jet impinge on a supersonic (Mach 2-3 at the nozzle exit) exhaust plume produced by expanding compressed air at room temperature through a converging-diverging (C-D) nozzle. The interaction results in the formation of a water spray whose break-up and flow characteristics are controlled by parameters relating to the air and water flows. The supersonic nature of the air jet and the ensuing spray formation require that non-intrusive diagnostics be utilized in the measurement setup. Introducing a probe in the flow-field can result in the formation of shock waves and distortion of the spray pattern resulting in altering the condition of interest. In this work, color Focusing Schlieren photography and laser sheet visualization are used to get a qualitative idea of the flow-field including the shock structure at the flow exit from the nozzle and in the vicinity of water injection. Phase Doppler Particle Anemometry (PDPA) is used for quantitative measurements of water droplet size and velocity at various locations in the spray. Moving forward, the same diagnostic tools will be used to examine more complex interactions of water sprays with the combusting flow of a gaseous oxygen hybrid rocket utilizing hydroxyl-terminated polybutadiene (HTPB) as a fuel.

B. Experimental Setup

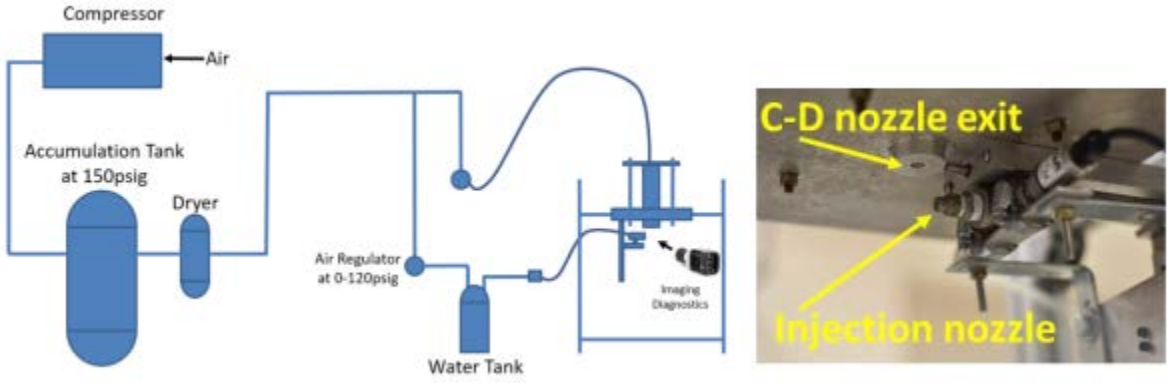

Figure 5: Left: Cold flow experimental diagram; Right: Photograph of the water injection system.

Figure 5 (*left*) shows a schematic of the experimental setup. Air from a compressor is fed through a dryer and regulated down to 150 psig before being supplied to a pressure chamber. A C-D nozzle is mounted at the bottom of the pressure chamber as shown in **Figure 5** (*right*). The air supply is also used to pressurize a tank containing water. The water tank is connected to an injection nozzle that injects a jet of water into the exhaust from the C-D nozzle. The injection nozzle is mounted on a traverse that allows the water jet to be injected at different downstream locations into the air flow. Air pressure is indicated by a gauge mounted on the pressure chamber. Water pressure is measured using a digital pressure transducer mounted just upstream of the injection nozzle. Temperatures of air and water are monitored using thermocouples. The

water flow rate is measured using a totalizing water flow meter. The C-D nozzle has an exit diameter of 9.65 mm (0.38”) and an area ratio of 2.25. Air expansion from a pressure of 150 psig in the nozzle to atmospheric conditions results in a Mach 2.8 flow at the nozzle exit. The water nozzle has an exit diameter of 1.52 mm (0.06”).

C. Experiment Parameters

Air pressure at the inlet to the chamber is maintained to be 150 psig for all the cases investigated in this work. Water pressure is varied between 20-80 psig. Several non-dimensionless groups can be calculated to characterize the experimental conditions. This includes the gas Weber (We_G) number, the Ohnesorge (Oh) number, momentum ratio (q), and the liquid jet Reynolds number (Re_l). For the conditions investigated in this work, Oh = 0.003 and We_G = 102,290. The other parameters for the various test conditions are summarized in ***Table 1***.

Table 1: Operating parameters for water corresponding to the different injection test cases.

Case #	Injection pressure [psig]	Jet speed, V_{jet} [m/s]	Momentum ratio, q	Reynolds number, Re_l
1	20	4.38	0.00397	6678
2	40	8.76	0.0159	13,355
3	60	13.14	0.0358	20,032
4	80	17.53	0.0636	26,710
5	100	21.91	0.0993	33,388

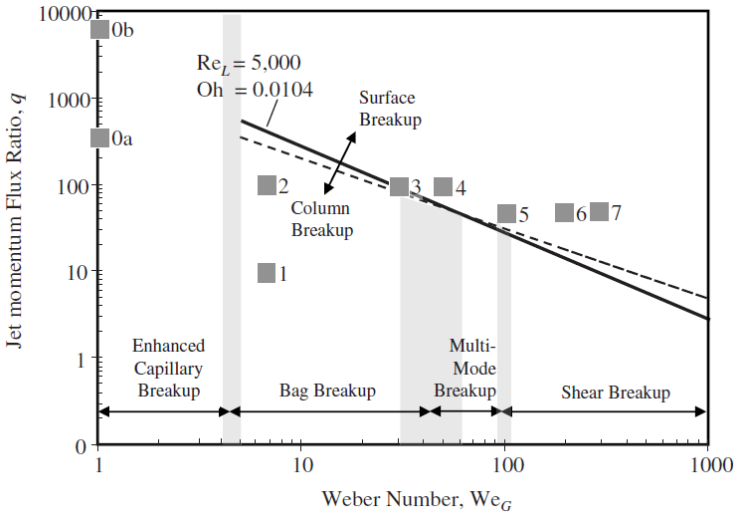

Figure 6: Regimes of liquid breakup processes [9].

Based on the gas Weber number and the momentum ratio, various regimes of liquid breakup processes in gas crossflow have been identified [9] as shown in **Figure 6**. **Figure 6** can be used to locate the test conditions of the current work with respect to the various liquid breakup processes explored in literature. As can be seen, the gas Weber number investigated in this work is almost an order of magnitude higher

than the range illustrated in **Figure 6**. Further, the current tests are performed at a very low momentum flux ratio given the large air jet velocity exiting the nozzle.

D. Experiment Diagnostics

The key phenomenon of interest in this work is the interaction of the supersonic air jet with the water jet and the ensuing spray formation. As mentioned previously, non-intrusive diagnostics are required to probe this interaction due to the supersonic nature of the air flow as well as the region of dense spray formed in the injection location. Both qualitative and quantitative measurements are of interest to provide data for validation of the numerical models. Three main diagnostics are utilized in this work to interrogate the region of interest: focused color Schlieren imaging of the air flow, laser sheet imaging of the water spray, high speed imaging with volume illumination, and PDPA for spray characterization.

The focused color Schlieren system is used to get a qualitative picture of the supersonic air flow exiting from the C-D nozzle. The FCS system utilizes a color-coded source image in place of a source grid in a traditional focusing Schlieren system. The focusing Schlieren itself is an improvement over traditional Schlieren which utilizes lenses and mirrors. **Figure 7** shows a schematic of the FCS system developed by Schoegl et al. and implemented in the current work. Further details of this technique can be found in the work by Schoegl et al. [10]. A Nikon D5600 digital SLR camera is used to capture the images in the FCS setup.

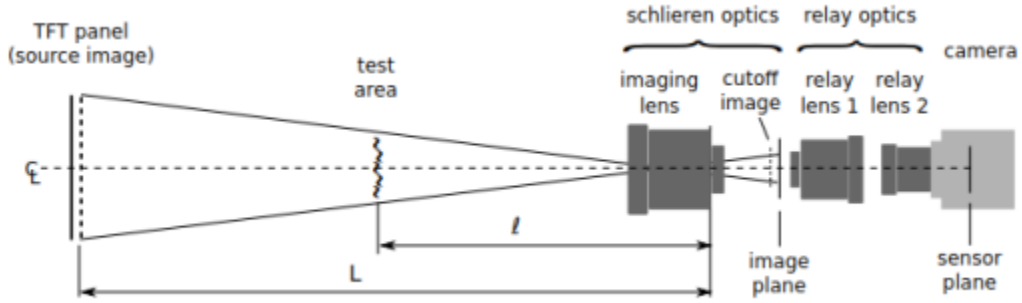

Figure 7: Schematic of the focusing color Schlieren system as employed in the current work [10].

A laser sheet is generated using the output from a pulsed Nd:YaG laser (New Wave Solo PIV) combined with a cylindrical lens. The laser provides 120 mJ/pulse at 532 nm with a 15 Hz pulse rate. The sheet is aligned with the center plane of the C-D nozzle and the injected water jet as shown in **Figure 8** (*left*). The sheet is imaged using a high speed camera (Photron SA-3) arranged at right angles to the laser sheet. The camera can be operated at 2,000 frames per second with a resolution of 1024x1024 pixels. It can also be operated at up to 120,000 frames per second with a reduced resolution. The camera is triggered using the synchronization pulse generated by the laser. The laser pulse width is 3-5 ns while the images are acquired at 60 frames per second giving a time scale of 17 ms. The same high speed camera is also used with volume illumination to obtain high speed videos of the spray breakup process. The setup for the high speed videos is similar to that shown in **Figure 8** (*left*) with halogen bulbs used to illuminate the spray from different directions instead of the laser sheet.

A two-component classic PDPA setup is used to measure water droplet sizes and velocities in the spray. A continuous Argon ion laser (Spectra-Physics Stabilite 2017) is used which is capable of emitting 1.5 W at 488 nm and 2 W at 514.5 nm. The green light at 514.5 nm is intended to measure the U component of velocity (vertical component) while the blue light (488 nm) is intended for V component of velocity (one of the components in the horizontal plane). In this work only the U component of velocity has been

measured. This was caused by difficulties in getting sufficient laser power at the 488 nm wavelength. **Figure 8** (*right*) shows the PDPA setup and **Table 2** summarizes the major operating parameters.

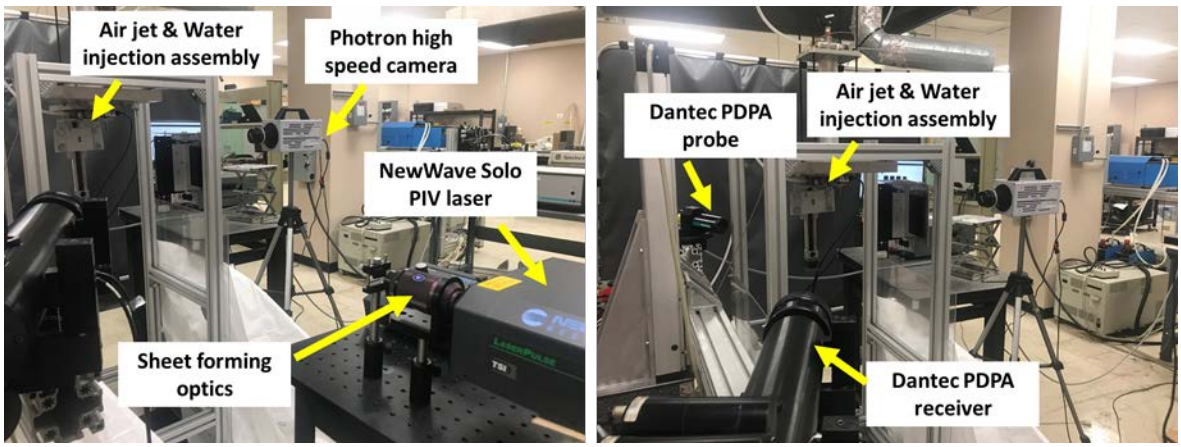

Figure 8: Experimental setups for the laser sheet imaging (left) and PDPA measurement (right).

Table 2: Parameters for the PDPA setup.

Parameter		Droplet Data	Units
Scattering angle		60	Degrees
Probe volume	x-dimension	0.1943	mm
	y-dimension	0.1941	mm
	z-dimension	4.091	mm
Number of fringes		35	
Fringe spacing		5.422	mu.m
Beam diameter		1.35	mm
Beam separation		38	mm
Transmitter focal length		400	mm
Receiver focal length		600	mm

III. Results & Discussion

I. Exhaust plume structure

A supersonic plume is formed at the exit of the C-D nozzle as seen in **Figure 9** (*left*), which shows the result as obtained from the focusing color Schlieren setup. For the operating conditions of the experiment (150 psig chamber pressure), the nozzle is overexpanded, resulting in the formation of oblique shock waves at the nozzle exit. A shock train develops consisting of alternating sets of oblique shock waves and expansion fans, each of which reflect off the free boundary surface. This flow structure is consistent with that of a supersonic overexpanded free jet. **Figure 9** (*middle*) shows a simulation result for iso-contours of Mach number obtained for conditions and geometry identical to that of the experiment. The simulation result shows some flow separation that begins slightly above the exit plane of the nozzle. The overexpansion of the flow is observed in the simulation result as well with the formation of oblique shocks close to the nozzle exit plane. This is followed by the shock train consisting of alternating expansion fans and oblique shock waves. The iso-contours of Mach number plotted in **Figure 9** (*middle*) indicate that the Mach number along the center line changes considerably as the flow proceeds downstream from the nozzle exit. Close to the exit plane, the Mach number is closer to about 3, which agrees well with the computed exit Mach

number of 2.8 based on the total pressure in the chamber and the nozzle area ratio. A DSLR camera is used to acquire images in the FCS setup and is operated with a frame rate of 60 frames/second. So the image observed in **Figure 9** (*left*) is time averaged over a period of about 17 ms. A characteristic flow time scale can be calculated using the jet exit velocity and the nozzle exit diameter as,

$$t_{flow} = \frac{d_{jet}}{u_{jet}} = \frac{0.00965}{608} = 16\ \mu s$$

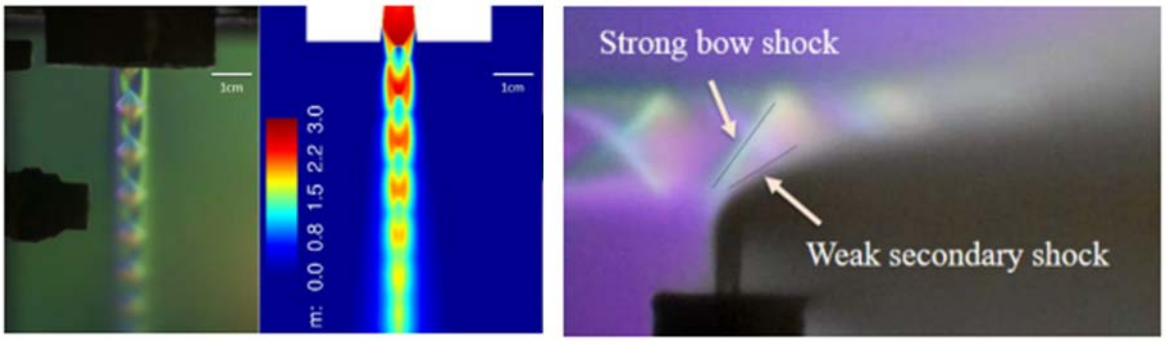

Figure 9: Left: FCS image showing air jet, Middle: CFD result for identical flow and geometry, Right: FCS image showing shock wave structure for low momentum ratio (q=0.002, Pinj~15 psi).

This indicates that the image acquired using the FCS setup is averaged roughly over 1000 flow time scales. Despite the averaging, the shock structure is observed to be very steady and past an initial start-up transient, moves very little in space. The Prandtl-Pack relationship can be used to estimate the shock cell spacing and is given by [11],

$$L_s = \pi\left(M_j^2 - 1\right)^{1/2} \frac{D_j}{\mu_1}, \text{ where } \mu_1 = 2.40483$$

Using the above relationship, the length of the shock cell is calculated as 32.9 mm. This does not agree well with the estimated shock cell length of 14.24 mm using the simulations and 14.24 mm using the experimental data.

Figure 9 (*right*) shows an image obtained from the FCS setup for a water injection pressure of about 15 psig. The changes in the shock structure due to the water injection process are well captured by the FCS imaging. A strong, stationary bow shock is formed upstream of the injection location. A weak secondary shock, which is harder to observe is also formed very close to the leading edge of the injection point. The strong bow shock is a distinctive feature which is observed for all the cases studied from ***Table 1***. The weak secondary shock is more obviously seen for the lower water injection pressure cases and is harder to detect at higher injection pressures. **Figure 9** (*right*) also appears to show the shock train being deviated slightly away from the injection plane past the injection location. No changes are observed in the shock train upstream of the injection location consistent with the supersonic nature of the flow. A significant difference between the current test configuration and the well-studied jet-in-crossflow is that there is no solid boundary constraining the air or liquid flows. This allows the injected water jet considerably more flexibility in the path it can take once it impinges on the air jet. It is highly likely also that part of the liquid jet might try to move around the periphery of the air jet without penetrating into it. This is not currently observable given our present diagnostics but is of interest to pursue in future experiments. Finally, the image in **Figure 9** (*right*) shows a fine spray being formed upon impingement of the water jet on the air jet. The structure of the spray will be described in the following section.

II. Water spray structure

The water jet results in a spray structure upon impingement with the air jet. The degree of breakup and ensuing atomization depends critically on the water injection pressure for a fixed air flow. For all the results presented in this work the injection location is maintained the same, at 25.4 mm below the exit plane of the C-D nozzle and 12.3 mm from the centerline of the injector. These dimensions are illustrated in the simulation result shown in **Figure 10**. The various locations can also be expressed in terms of the jet diameter as $\bar{x}/d_e$, where $\bar{x}$ is the downstream distance from the nozzle exit plane and d_e is the effective orifice diameter computed from the jet exit diameter (d_j) as [13],

$$d_e = {C_D}^{0.5} d_j$$

where C_D is the discharge coefficient of the nozzle equal to 0.7 for this case. The injection location corresponds to 20 jet diameters ($\bar{x}/d_e = 20$) downstream of the C-D nozzle exit plane. **Figure 10** also shows the locations where PDPA measurements were obtained as will be discussed in the next section.

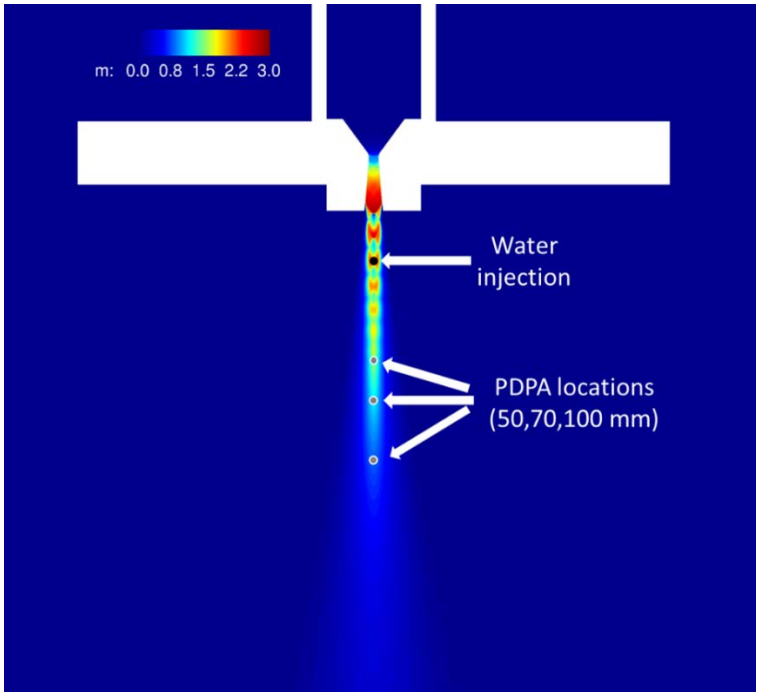

Figure 10: CFD simulation result showing Mach number contours overlaid with water injection and PDPA probe locations.

Table 3: Significant locations in the experimental configuration.

Location	Distance from nozzle exit plane (mm)	$\bar{x}/d_e$
Water injection	25.4	20
PDPA probe location # 1	75.4	59
PDPA probe location # 2	95.4	75
PDPA probe location # 3	125.4	98

Figure 11 shows a series of images obtained using the laser sheet illuminated imaging approach as shown in **Figure 8** (*left*). Results are shown for all five water injection pressures as presented in ***Table 1***.

Each image represents the mean over 3 separate images. **Figure 12** shows a similar result, however in that case, each image represents the mean over 5 separate images. It should be noted that the laser pulse width is 3-5 ns while the images were acquired at 60 frames per second with an exposure time of 16.67 ms. Given that the flow time scale is of the order of 16 μs, the images are averaged over about 1000 flow time scales. The results can be improved in the future by reducing the camera exposure as close as possible to the laser pulse width to get a nearly flowfield. While not instantaneous, the images still provide a good qualitative picture of the spray pattern that develops following the impingement of the water jet. Each of the individual images in **Figure 11** and **Figure 12** also shows a dashed line representing the centerline of the nozzle.

The key effect of increasing the water injection pressure is changing the jet penetration height. At 20 psi injection pressure, the water jet barely moves into the air jet and is almost vertical in shape once the flow is turned by the air jet. This changes with increasing water injection pressure as the jet penetrates more and more into the air jet. For the case of 100 psi injection pressure, the water jet is seen to completely penetrate through the air jet. The brighter areas in the images in **Figure 11** and **Figure 12** are indicative of a higher water spray density. The reason for presenting two sets of images in **Figure 11** and **Figure 12** representing averages over different number of images was to attempt to see whether any periodic large-scale coherent structures could be observed in the spray. As seen using high speed video, the flow-field itself is highly transient particularly in the locations considerably downstream of the injection location. However, no coherent structures are clearly seen in the time-averaged images. Future investigations will attempt to use particle image velocimetry (PIV) using the water droplets as seed particles to investigate the velocity field.

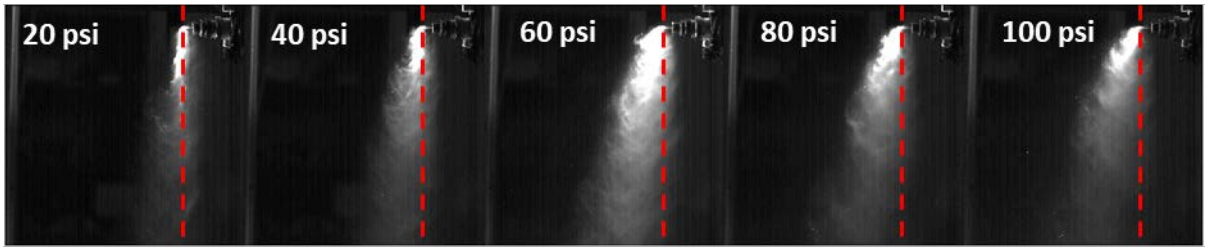

Figure 11: Averaged laser sheet illuminated images showing water jet interaction at different injection pressures.

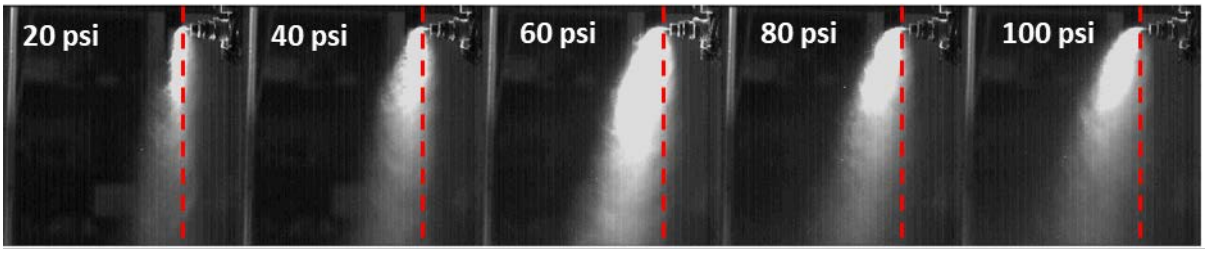

Figure 12: Averaged laser sheet illuminated images showing water jet interaction at different injection pressures.

The jet penetration height is an important quantity for which a number of analytical correlations have been proposed. In this work, the penetration height as a function of axial location is extracted from the high speed images obtained with volume illumination. The images are processed using the Savitzky-Galoy filter and a 7% transmission rule [12] is used to identify the jet penetration height. **Figure 13** shows an image after the filtering operation for a case of 60 psi water injection pressure. **Figure 14** shows the penetration

height plotted as a function of the downstream distance. The experimentally measured values are compared to a correlation by Yates [13] given by,

$$\frac{\bar{y}_B}{d_e} = 1.1q^{0.5} ln\left(1 + 10\frac{\bar{x}}{d_e}\right)$$

where $\bar{y}_B$ is the vertical distance from the injection plane along the jet boundary, d_e is the effective orifice diameter, and $\bar{x}$ is the downstream distance from the center of the injector.

Figure 13: Averaged image after filtering for a case of 60 psi injection pressure as used to extract the penetration height.

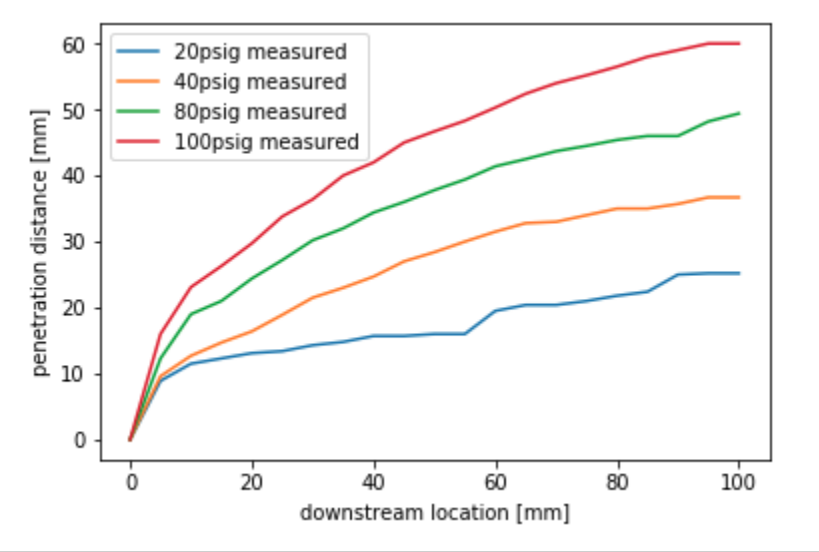

Figure 14: Jet penetration height extracted for the different water injection cases from the high speed volumetrically illuminated images.

The equation is predicted to hold for downstream regions more than 10 effective jet diameters from the injection location, ($\bar{x}/d_e > 20$). The agreement between the measured experimental data and the Yates' correlation is found to be very poor. The correlation greatly underpredicts the measured data. While this issue needs to be investigated further, the discrepancy is likely due to the significantly different nature of crossflow investigated in the current work as opposed to a conventional jet-in-crossflow for which the Yates' correlation was derived. The air jet diameter is about 6.3 times the diameter of the water jet. This

ratio is significantly smaller than the ratio of the channel height to jet diameter for the jet-in-crossflow configuration, which tends to be around 100 or higher. This implies that for the current configuration, the ability of the air jet to entrain and move the water spray downstream is limited due to its size. This issue will be further investigated in future work.

III. Water spray characteristics

The PDPA setup illustrated in **Figure 8** (*right*) was used to obtain quantitative measurements in the water spray. One component velocity (vertical) and droplet size distributions were obtained along the centerline of the air jet. Measurements were obtained at various locations starting from 45 mm ($\bar{x}/d_e = A$) below the C-D nozzle exit plane to 100 mm ($\bar{x}/d_e = A$) below the exit plane. **Figure 15** and **Figure 16** show the results from the PDPA measurements for velocity and droplet size distributions respectively. Results are presented in the form of histograms for three water injection pressures (20, 40, and 80 psi) and at three locations downstream from the C-D nozzle exit plane (50, 70, and 100 mm). The distributions are primarily of a skewed nature and skewed to the right.

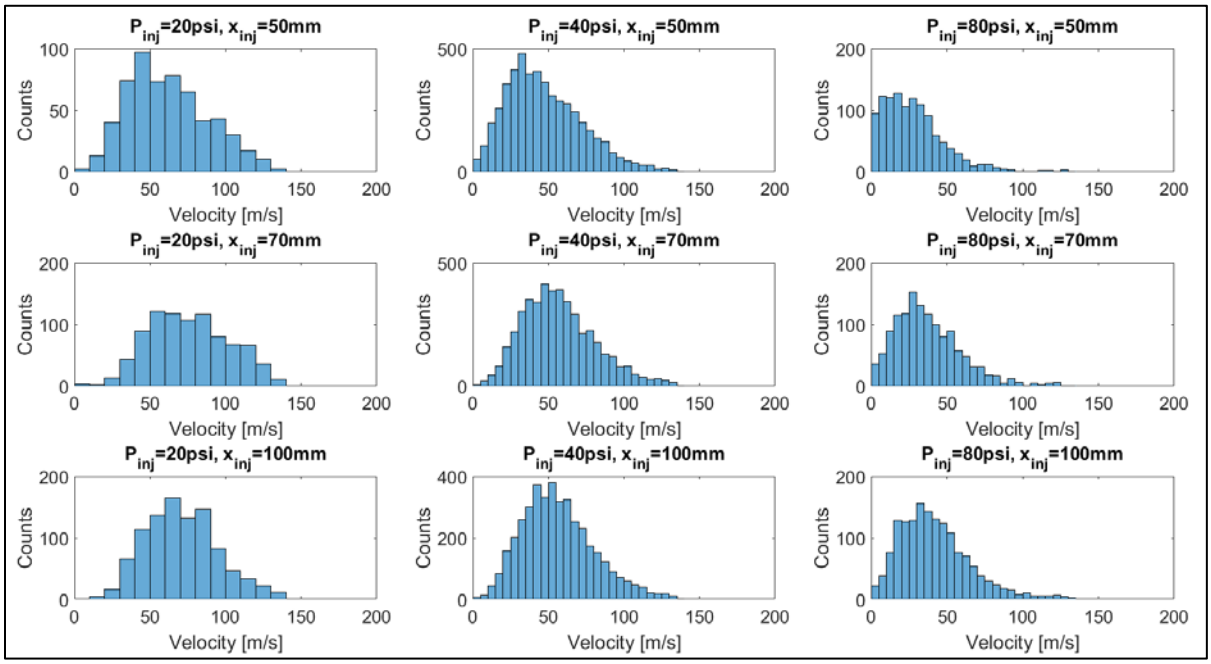

Figure 15: Histograms showing droplet velocity distributions at various injection pressures and locations downstream of the injection location.

Figure 15 shows histograms for the downstream component of the droplet velocities with values ranging from 0 to about 150 m/s depending on the specific case. Considering the effect of increasing pressure, at a fixed location of 50 mm (top row of **Figure 15**), it is observed that while the peak velocity for the 20 psi injection case is around 50 m/s, the same value shifts to a lower magnitude for the 40 psi (~30 m/s) and 80 psi (~25 m/s) cases. This is explained by the fact that for the same air flow velocity in all three cases, the air flow has to expend more momentum to break up the water jet and turn the spray to make it move in a downward direction. Since the water jet momentum increases with increasing injection pressure, the induced velocity of the water spray droplets decreases for a constant air flow. Additionally, this shift in droplet velocity can be attributed to increased deformation of the mean liquid flow at increased pressure. The liquid stream is turned away from the centerline of the gas jet where measurements are taken, further

decreasing the measured velocity. Considering the same injection pressure but moving to downstream locations, the velocity is observed to increase. This is indicated by the histograms shifting towards the right in each column shown in **Figure 15**. This is caused by the acceleration of the entrained droplets by the air flow given that its momentum is between one to two orders of magnitude greater than that of the water jet as listed in ***Table 1***. The acceleration of the entrained droplets is most evident while comparing the cases for each water injection pressure at 50 and 70 mm downstream from the exit of the C-D nozzle. From 70 to 100 mm, the acceleration is not as evident likely due to the continuous drop in air flow Mach number as the supersonic jet dissipates energy in the ambient environment resulting in a corresponding decrease in the momentum of the air flow.

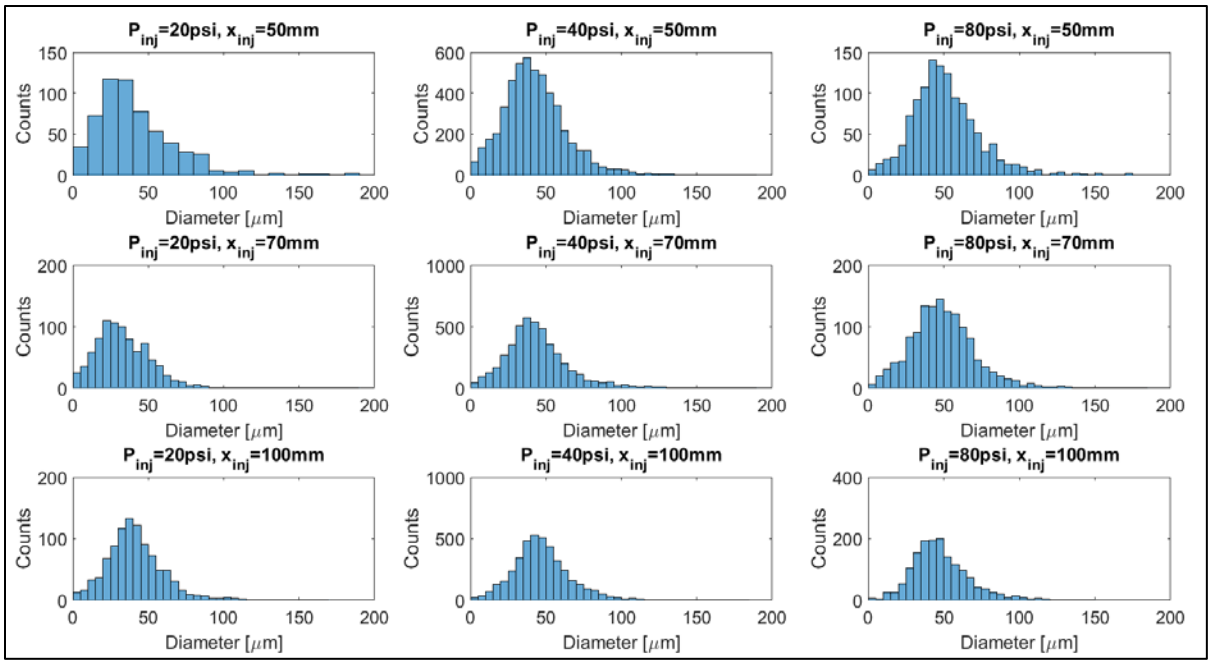

Figure 16: Histograms showing droplet diameter distributions at various injection pressures and locations downstream of the injection location.

Considering the droplet size distributions shown in **Figure 16**, the sizes range from 0 to 100 µm depending on the specific case. As noted in **Table 2**, the biggest droplet that can be captured using the current PDPA settings has a diameter of about 180 µm. For the fixed observation location of 50 mm, the effect of increasing the injection pressure is to shift the histogram to the right and increase the average size of the droplets. The distribution is also seen to become somewhat narrower. For the large Weber number, low momentum ratio cases investigated in this work, the primary mechanism for the jet breakup is through aerodynamic shattering. As the injection pressure is increased, the higher momentum water jet becomes less susceptible to shattering, resulting in the formation of larger droplets, and thus shifting the distribution of the histograms towards the right. Once the droplets are formed and entrained in the air flow, given the ambient temperatures at which the tests are carried out, there are no significant mechanisms for reducing the size of the droplets such as evaporation. This suggests that the droplet size distribution might stay the same for the same injection pressure as the observation moves to different downstream locations (following a column of pictures in **Figure 16**). However, the distribution is observed to become somewhat narrower and there is a slight shift in the histograms towards the right. This might be caused by the motion of smaller droplets away from the centerline as the jet expands due to the growth of the shear layer as well as off-axis air flow that may be induced by the outer boundaries of the experiment. Larger droplets having a bigger

momentum might be able to stay along the centerline even as smaller droplets are moved out. This can be further investigated using either simulation results or experimental results obtained using PIV.

IV. Conclusions

The proper use of computational codes such as the one in use at NASA' s Stennis Space Center which is used to inform analysis decisions regarding the design of test hardware used for the testing of rocket engines requires validation to ensure confidence in proper results. Further, more investigation is required on aspects of the water jet injection process such as injection location and water pressure that can optimize achieved plume cooling and noise suppression effects. To this effect, a scaled testing facility is being developed and utilized to provide subscale validation data for this code.

In the present work, the test facility has been operated with cold flow generating a supersonic flow of air by expanding compressed air through a converging-diverging nozzle. A jet of water is injected into the air flow and the subsequent interaction of the two jets are studied using non-intrusive diagnostics. The diagnostics include a focusing color Schlieren setup to look at the supersonic air flow, a high speed camera to study the spray, which is illuminated by a laser sheet as well as in a volumetric manner using halogen bulbs, and finally a Phase Doppler Particle Anemometer for quantitative measurements of the water spray.

The exhaust plume structure is observed to be that of an overexpanded free jet whose structure agrees well with predictions from a simulation model. A bow shock is observed to be formed for all the cases investigated just upstream of the injection location along with a weak secondary shock wave close to the leading edge of the injection point. The water spray is observed to vary depending on the injection pressure. By increasing injection pressure from 20 to 100 psi, the water jet can be made to completely break through the supersonic air jet. Images from the high speed video are used to extract the penetration height. The measured penetration height is considerably underpredicted by established correlations for jet-in-crossflow configurations. This is likely due to significantly higher value of the ratio of the air jet diameter to that of the water jet. Water droplet velocity and size distributions were obtained using the PDPA setup for different injection pressures and at various downstream locations from the air nozzle exit plane. The behavior of the histograms are analyzed and explained with respect to the changes in injection pressure and observation location.

Overall, an extensive amount of qualitative and quantitative information is extracted for the interaction of a cold supersonic flow with an impinging water jet. This data will be used to validate results from currently ongoing simulations of the experimental setup. The data will be supplanted in the future with particle image velocimetry measurements using the water drops as seed particles. Finally, the experiments will be further extended to a hot combusting flow by replacing the current compressed air chamber by a scaled hybrid rocket engine.

V. Acknowledgements

This work is supported by NASA EPSCoR and the Board of Regents of the state of Louisiana through the Research Award Program as well as the Graduate Student Research Assistance Award. We would like to thank Dr. Daniel Allgood from NASA Stennis Space Center for his support and collaboration. We would also like to thank Dr. Ingmar Schoegl from LSU for use of the focusing color Schlieren apparatus developed by him and his research group.

VI. References

[1] Sachdev, J. S., Ahuja, V., Hosangadi, A., and Allgood, D. C., "Analysis of Flame Deflector Spray Nozzles in Rocket Engine Test Stands," 46th AIAA/ASME/SAE/ASEE Joint Propulsion Conference & Exhibit, Nashville, TN, 2010.

[2] Bauer, C., Koch, A., Minutolo, F., and Grenard, P., "Engineering model for rocket exhaust plumes verified by CFD results," 29th ISTS meeting, Nagoya, Japan, 2013.

[3] Allgood, D. and Ahuja, V., "Computational plume modeling of conceptual ares vehicle stage tests," 43rd AIAA/ASME/SAE/ASEE Joint Propulsion Conference & Exhibit, Cincinnati, OH, 2007.

[4] Jones, D. R., Allgood, D. C., & Saunders, G. P. (2016). Passive Rocket Diffuser Testing: Reacting Flow Performance of Four Second-Throat Geometries.

[5] Kumaran, R. M., Sundararajan, T., & Manohar, D. R. (2010). Performance Evaluation of Second-Throat Diffuser for High-Altitude-Test Facility. Journal of Propulsion and Power, 26(2), 248-258.

[6] Ferrell, J. (1967). Simulated Space Testing of Propulsion Units and Systems.

[7] Project Morpheus. (n.d.). Retrieved January 4, 2018, from https://en.wikipedia.org/wiki/Project_Morpheus

[8] Allgood, D., Saunders, G., and Langford, L., "Reduction of altitude diffuser jet noise using water injection," 50th AIAA Aerospace Sciences Meeting including the New Horizons Forum and Aerospace Exposition, Nashville, TN, 2010.

[9] Arienti, M., & Soteriou, M. C. (2009). Time-resolved proper orthogonal decomposition of liquid jet dynamics. Physics of Fluids, 21(11), 112104.

[10] Schoegl, I., Pisano, A. J., & Sedky, G. (2016). Development of a compact focusing color schlieren technique. In 54th AIAA aerospace sciences meeting, San Diego, CA, USA, AIAA (Vol. 1765).

[11] Munday, D., Gutmark, E., Liu, J., & Kailasanath, K. (2011). Flow structure and acoustics of supersonic jets from conical convergent-divergent nozzles. Physics of Fluids, 23(11), 116102.

[12] Lin, K. C., Lai, M. C., Ombrello, T., & Carter, C. D. (2017). Structures and Temporal Evolution of Liquid Jets in Supersonic Crossflow. In 55th AIAA Aerospace Sciences Meeting (p. 1958).

[13] Yates, C. (1971). Liquid injection into supersonic airstreams. In 7th Propulsion Joint Specialist Conference (p. 724).